Article:
Kim, J orcid.org/0000-0002-3456-6614 and Kadem, O (2023) Real-Time State of Charge-Open Circuit Voltage Curve Construction for Battery State of Charge Estimation. IEEE Transactions on Vehicular Technology, 72 (7). 8613 -8622. ISSN 0018-9545

https://doi.org/10.1109/TVT.2023.3244623

Real-Time State of Charge-Open Circuit Voltage Curve Construction for Battery State of Charge Estimation

Onur Kadem and Jongrae Kim, *Senior member, IEEE*
Institute of Design, Robotics, & Optimisation (iDRO)
School of Mechanical Engineering, University of Leeds, Leeds LS2 9JT
United Kingdom [e-mail: (mn16ok, menjkim)@leeds.ac.uk]

***Abstract*—All state of charge (SoC) estimation algorithms based on equivalent circuit models (ECMs) estimate the open circuit voltage (OCV) and convert it to the SoC using the SoC-OCV nonlinear relation. These algorithms require the identification of ECM parameters and the nonlinear SoC-OCV relation. In literature, various techniques are proposed to simultaneously identify the ECM parameters. However, the simultaneous identification of the SoC-OCV relation remains challenging. This paper presents a novel technique to construct the SoC-OCV relation, which is eventually converted to a single parameter estimation problem. The Kalman filter is implemented to estimate the SoC and the related states in batteries using the proposed parameter estimation and the SoC-OCV construction technique. In the numerical simulations, the algorithm demonstrates that it accurately estimates the battery model parameters, and the SoC estimation error remains below 2%. We also validate the proposed algorithm with a battery experiment. The experimental results show that the error in SoC estimation remains within 2.5%.**

***Index Terms*—electric vehicles; state of charge estimation; adaptive systems; nonlinear filters; stochastic systems.**

I. Introduction

Lithium-ion batteries are successfully employed in many devices as a power source. Their high energy density and long lifespan make them more attractive among the different battery types [1], [2], [3]. However, overcharging or discharging lithium-ion batteries shortens their lifespan and irreversibly damages their performance. Thus, monitoring the battery states with high accuracy is critical in the design of battery management systems (BMSs).

Today, lithium-ion batteries are increasingly used to power electric vehicles (EVs) due to the aforementioned advantages. EV producers must assure the safe application, enhance the driving range, optimise the power management strategy, prolong the service life and reduce the cost of the batteries. A reliable BMS is necessary to fulfill multiple tasks including the fault diagnosis, estimation of the battery state of health (SoH) and state of charge (SoC). Battery fault diagnosis is important for the safe operation of the batteries. In the majority of the existing literature, the battery fault is diagnosed based on the battery voltage and temperature. An alternative method based on the battery charging capacity is proposed in [4]. Real-time SoH estimation requires comprehensive and labor-intensive laboratory tests. SoH estimation method based on incremental capacity analysis has been proposed in [5]. The SoC is the most important indicator to make charge or discharge decision and assure the battery's safety, efficiency, and longevity. As a result, investigations about accurate SoC estimation techniques are the center of researches in improved BMS design tasks.

Battery SoC determination is always a primary function of a BMS. Therefore, a large number of methods have been proposed to estimate the battery SoC in real-time. These methods can be classified into two groups: the model-free approaches and the model-based approaches [6], [7], [8]. Coulomb counting (CC) and open circuit voltage (OCV) measurement methods are two common model-free approaches. The CC method measures the battery's charging/discharging current and integrates it over time to estimate the SoC [9]. However, it is not only sensitive to the unknown initial SoC value but also accumulates error from the current measurement sensor over time because of the integration process [10]. The OCV measurement method provides accurate SoC estimations but it requires a look-up table for the SoC-OCV relationship [11]. Once the OCV is measured, the corresponding SoC can be easily found from the look-up table. However, accurate measurement of the OCV requires a long relaxation time in the range of hours and this is not suitable for online applications [12].

The model-based methods are constructed in a closed-loop structure, which continuously reduces the error in SoC estimation using the available current and voltage measurements, and it leads to a better SoC estimation. The model-based approaches describe the battery dynamics in two different ways of battery modelling, i.e., the electrochemical models and equivalent circuit models (ECMs).

The electrochemical models use several coupled differential equations to describe the electrochemical process in the battery [13]. The most popular electrochemical models are the pseudo-two-dimentional (P2D) model and single particle model (SPM). The P2D model is based on the porous electrode theory, the concentrated solution theory and the kinetics equations [14]. However, its usage is not preferred in state estimation due to its complexity. As such, the SPM

(*Corresponding author: Onur Kadem.*)

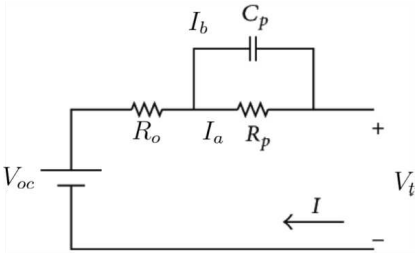

Fig. 1: First order Equivalent Circuit Model for the Battery

has been developed to simplify the P2D model. In the SPM, two assumptions are made to approximate each electrode as a single spherical particle. Firstly, the electrodes are assumed to be composed of multiple uniform sized spherical particles, followed by the current distribution being uniform along the both electrodes [15], [16]. However, the solutions to the differential equations and parametric uncertainties in these models remain a challenge to solve [17], [18].

Thevenin-based ECMs are widely employed in online BMS applications [8], [19], [20], [21]. Thevenin-based ECMs do not require thorough knowledge about battery electrochemistry, and they provide a good description of battery dynamics [8], [19]. This advantage of ECMs makes them easily adapted to estimation and control algorithms and implementation in embedded micro-controllers compared to the electrochemical models. Thus, the ECMs based methods lead the real time estimations such as the Kalman filter (KF) in [22], extended Kalman filter (EKF) in [23], unscented Kalman filter (UKF) in [24] and particle filter (PF) in [25], [26].

The ECM consists of basic circuit elements including resistors, capacitors and voltage source as shown in Figure 1. Most SoC estimation algorithms must run on a battery model whose parameters are known. This implies that a parameter identification procedure is necessary to prepare the model for SoC estimation. The battery model parameters can be identified through either offline or online. Offline parameter identification is a heavily laborious experimental task. Although a set of batteries can originate from the same production line, deviations in parameter values between the batteries are natural. Thus, an experiment has to be conducted for each battery. Moreover, the experimental conditions and battery ageing also affect the parameter values.

The online parameter estimation is appropriate to adapt to varying conditions. There are different approaches to estimate the parameters online. In [27], the model parameters are added as states into the state vector and estimated using the adaptive UKF. Recursive least square (RLS) algorithms are commonly used in battery model parameter estimation [21], [28], [29], [30], [31]. However, the convergence and the stability of the proposed RLS techniques cannot be guaranteed. In [32], the proposed methodology uses the adaptive control theory to estimate the battery model parameters on-line so that the convergence and stability of the estimator are guaranteed. However, in a typical parametric model, the parameter vector includes battery model parameters along with the OCV as a function of SoC. This may cause inaccurate SoC estimation since the model parameters may not converge to their true values.

The nonlinear SoC-OCV relation is commonly assumed to be known and is used to map a value of OCV to its corresponding SoC value. However, the true SoC-OCV relation changes due to battery ageing and temperature change. This difference is directly reflected as an error in SoC estimation [33]. Similar to the parameter estimation, the SoC-OCV relation could be obtained through an experimental procedure [34], [35], [36], which is vulnerable to a change in operational conditions. The effect of SoC-OCV model and characterisation tests the accuracy of SoC estimation is investigated in [37]. Different types of tests are performed to acquire the SoC-OCV characteristic depending on various operational conditions. However, this relation is unique for a specific battery used during the test and cannot apply to different batteries and conditions. The SoC-OCV curve at different temperatures is identified offline and mapped by using the polynomial electrochemical equation in [38]. The equation does not consider the effect of battery ageing on the SoC-OCV curve, which deteriorates the accuracy of SoC estimation eventually. In [39], the curve is obtained by sorting the estimated OCV according to SoC calculated using CC technique. However, it is expected that the accuracy of the curve decreases with time since the CC technique stores the error at each calculation step. In [40], the relation is modelled by using piece-wise linear functions and it is assumed that SoC-OCV relation is fixed, which does not take into account the changes in the true relation.

We propose an adaptive estimation algorithm for the SoC with a nonlinear SoC-OCV curve. The algorithm estimates the parameters describing the ECM and the SoC-OCV curve. Unlike other algorithms, the proposed method does not require high experimental labour. In addition, the algorithm automatically adapts to changes in operational conditions and battery ageing without requiring any manual adjustments.

The organisation of the paper is as follows: Section II introduces the battery model; Section III presents the parameter estimation; Section IV summarises the OCV estimation; Section V explains the the SoC-OCV curve estimation method; Section VI shows simulation results to demonstrate the efficiency of the proposed method; Section VII shows the experiment results; finally, conclusions and future works are discussed in Section VIII.

II. Lithium battery modelling

A reliable battery model should have low complexity yet be able to describe the battery dynamics. Various battery technologies including lithium-ion battery technologies use and adopt resistor-capacitor (RC)-equivalent circuit models for real time utilisation. To prevent the large matrix operations, the first-order RC model is the best candidate to accurately represent the system's dynamics in lithium-ion battery applications [41], [42], [43], [44].

Figure 1 shows the first-order RC model of a lithium battery, which consists of a standard parallel 1-RC branch and an internal resistor, R_0, which causes an energy loss during charging or discharging phases. The battery's transient and relaxation responses, which occur during or after

the charging/discharging cycles, are modelled by the parallel RC branch. R_p and C_p are the polarisation resistance and capacitance, respectively. R_0, R_p and C_p vary according to the ambient temperature and battery ageing even at the same SoC levels. The terminal voltage, V_t, converges to its steady state voltage, which is the OCV, V_{oc}, if the load is removed from the battery for sufficiently enough time, e.g., 1 hour.

I is the current flowing across the battery's poles and I is positive on discharge or negative on charge. I is divided into I_a that flows over R_p and I_b that flows over C_p. The following equations express the battery transient response:

$$\dot{I}_a = -\frac{I_a}{\tau} + \frac{I}{\tau} \tag{1a}$$

$$V_t = V_{oc} - I_a R_p - I R_0 \tag{1b}$$

where $\dot{(\cdot)} = d(\cdot)/dt$ and $\tau = R_p C_p$. The measurable states of the battery are V_t and I. As the polarisation voltage, V_p, across the RC branch is equal to $I_a R_p$, the differential equation for V_p is obtained as follows:

$$\dot{V}_p = -\frac{V_p}{\tau} + \frac{I}{C_p} \tag{2a}$$

$$V_t = V_{oc} - V_p - I R_0 \tag{2b}$$

which gives the common expression for the battery dynamics [45], [12]. In (2b), V_{oc} refers to a nonlinear function of SoC. The SoC-OCV model is required to transform the OCV to the SoC.

The chemical reactions in the battery dynamic process are affected by the ambient temperature and battery ageing. Consequently, the battery parameters, i.e., R_0, R_p, C_p and the SoC-OCV model vary in time. R_0, R_p and C_p are to be estimated in the next section and then the SoC-OCV model is to be built in Section V.

III. Battery Parameter Estimation

Discretise (2)

$$V_{p,k+1} = \beta V_{p,k} + (1-\beta) R_p I_k \tag{3a}$$

$$V_{t,k} = V_{oc,k} - V_{p,k} - R_0 I_k \tag{3b}$$

where $(\cdot)_k$ is the k^{th} sample of $(\cdot)$, $\beta = e^{-\Delta t_s/\tau}$ and Δt_s is the sampling time. Rewrite (3b) for step $k+1$

$$V_{t,k+1} = V_{oc,k+1} - V_{p,k+1} - R_0 I_{k+1} \tag{4}$$

Substituting (3a) into (4)

$$V_{t,k+1} = V_{oc,k+1} - \beta V_{p,k} - (1-\beta) R_p I_k - R_0 I_{k+1} \tag{5}$$

Rearrange (3b) and substitute into (5)

$$\begin{aligned} V_{t,k+1} =& \beta V_{t,k} - R_0 I_{k+1} + \left[\beta R_0 + (\beta-1) R_p\right] I_k \\ &+ V_{oc,k+1} - \beta V_{oc,k} \end{aligned} \tag{6}$$

Define

$$\Delta V_{t,k+1} = V_{t,k+1} - V_{t,k} \tag{7}$$

Substitute (6) into (7) for k and $k+1$ sampling time

$$\begin{aligned} \Delta V_{t,k+1} =& \beta \Delta V_{t,k} - R_0 \Delta I_{k+1} + \gamma \Delta I_k \\ &+ \Delta V_{oc,k+1} - \beta \Delta V_{oc,k} \end{aligned} \tag{8}$$

where $\Delta(\cdot)_{k+1} = (\cdot)_{k+1} - (\cdot)_k$ and $\gamma = \beta R_0 + (\beta - 1) R_p$. V_{oc} is known to vary slowly compared to V_t, and the change in V_{oc} is assumed to be negligible during the sampling interval [46]. Equation (8) is approximated as

$$\Delta V_{t,k+1} = \beta \Delta V_{t,k} - R_0 \Delta I_{k+1} + \gamma \Delta I_k \tag{9}$$

and it is written in a linear parametric model as follows:

$$y_{k+1} = \boldsymbol{\theta}_{k+1}^T \boldsymbol{\phi}_{k+1} \tag{10}$$

where the unknown parameters to be estimated are

$$\boldsymbol{\theta}_{k+1} = \begin{bmatrix} \beta & -R_0 & \gamma \end{bmatrix}^T \tag{11}$$

and the state vector is given by

$$\boldsymbol{\phi}_{k+1} = \begin{bmatrix} \Delta V_{t,k} & \Delta I_{k+1} & \Delta I_k \end{bmatrix}^T \tag{12}$$

As the terminal voltage is measured, the terminal voltage difference is obtained from two measurement samples. The measurement equation for the parameter estimation is defined by

$$\tilde{y}_{k+1} = \Delta V_{t,k+1} + e_{k+1} \tag{13}$$

where e_{k+1} is the measurement noise.

Now, one of the standard online parameter estimation algorithms based on adaptive law can be applied as follows [47]:

$$\varepsilon_{k+1} = \tilde{y}_{k+1} - \hat{\boldsymbol{\theta}}_k^T \boldsymbol{\phi}_{k+1} \tag{14a}$$

$$\hat{\boldsymbol{\theta}}_{k+1} = \hat{\boldsymbol{\theta}}_k + \Gamma \Delta t_s \varepsilon_{k+1} \boldsymbol{\phi}_{k+1} \tag{14b}$$

where $\hat{(\cdot)}$ is the estimate of $(\cdot)$, and Γ is the positive-definite adaptive gain matrix.

Once the estimation, $\hat{\boldsymbol{\theta}}_{k+1}$, is available, the parameters in the model are obtained by

$$\hat{R}_0 = -\hat{\theta}_{k+1}^{(2)} \tag{15a}$$

$$\hat{R}_p = \frac{\hat{\theta}_{k+1}^{(3)} + \hat{\theta}_{k+1}^{(1)} \hat{R}_0}{1 - \hat{\theta}_{k+1}^{(1)}} \tag{15b}$$

$$\hat{C}_p = \frac{-\Delta t_s}{\hat{R}_p \log \hat{\theta}_{k+1}^{(1)}} \tag{15c}$$

where $(\cdot)^{(i)}$ for $i = 1, 2, 3$ is the i^{th} element of $(\cdot)$.

IV. OCV Estimation Using Kalman Filter

The KF solves linear optimal estimation problems. As V_{oc} slowly varies in most of the practical cases, it is assumed to be a piece-wise constant, hence

$$V_{oc,k+1} = V_{oc,k} + w_{V_{oc},k} \tag{16}$$

where $w_{V_{oc},k}$ is the zero-mean Gaussian random process noise. The propagation of the current, I_a, is given by

$$I_{a,k+1} = \hat{\beta}_k I_{a,k} + \left(1 - \hat{\beta}_k\right) I_k + w_{I_a,k} \tag{17}$$

where $\hat{\beta}_k = \hat{\theta}_k^{(1)}$, $w_{I_a,k}$ is the zero-mean Gaussian random process noise. $w_{V_{oc},k}$ and $w_{I_a,k}$ are independent to each other. Equations (16) and (17) are the governing state-space equations. The measurement equation is given by

$$\tilde{V}_{t,k} = V_{oc,k} - I_{a,k} \hat{R}_p - I_k \hat{R}_0 + v_{y,k} \tag{18}$$

where $\tilde{V}_{t,k}$ is the measured terminal voltage, I_k is the charging or discharging terminal current at k-th sample and $v_{y,k}$ is the measurement noise. In a compact form,

$$\begin{aligned} x_{k+1} &= A_k x_k + B_k u_k + w_{x,k} \\ y_k &= C_k x_k + D_k u_k + v_{y,k} \end{aligned} \tag{19}$$

where

$$\begin{aligned} &x_k = \begin{bmatrix} I_{a,k} & V_{oc,k} \end{bmatrix}^T, \ y_k = \tilde{V}_{t,k}, \ u_k = I_k \\ &A_k = \begin{bmatrix} \hat{\beta}_k & 0 \\ 0 & 1 \end{bmatrix}, \ B_k = \begin{bmatrix} 1-\hat{\beta}_k \\ 0 \end{bmatrix}, \ w_{x,k} = \begin{bmatrix} w_{V_{oc},k} \\ w_{I_a,k} \end{bmatrix} \\ &C_k = \begin{bmatrix} -\hat{R}_p & 1 \end{bmatrix}, \ D_k = -\hat{R}_0, \end{aligned} \tag{20}$$

the covariance of $w_{x,k}$ is Q and the variance of $v_{y,k}$ is r. Note that the measurement noise is independent from the process noise.

V. SoC-OCV Estimation

ECM based SoC estimation applications use the SoC-OCV nonlinear relation to transform the estimated OCV to a SoC estimation. This relation is unique for every battery but sensitive to the ambient temperature and battery ageing. Hence, a relation that is obtained offline cannot be used for different batteries, testing protocols and operational conditions. Therefore, an online method is proposed to establish the SoC-OCV relation. The proposed method obtains the SoC-OCV relation by establishing a parameter estimation problem.

In general, the slopes of the SoC-OCV curve change drastically from the low values to the high values. The nonlinear function must be a one-to-one increasing nonlinear function as SoC increases. Firstly, the potential candidate model of the SoC-OCV relationship must meet these two requirements. Secondly, the number of model parameters to be identified must not be more than three. The latter requirement allows us to estimate the model parameters in real-time based on the boundary conditions and measurements. Considering these two requirements, we establish the following novel nonlinear model to capture these characteristics with three modelling parameters:

$$V_{oc} = a\log(z) + be^{z^3} + c \tag{21}$$

where a, b and c are the coefficients to be estimated, which are different for every battery and vary for each condition, z is the SoC in $[\delta, 1]$ and δ is a small positive number. The SoC below δ is considered to be zero. This nonlinear equation expresses the typical shape of the SoC-OCV curve and their variations. By estimating the three parameters, the estimated SoC-OCV curve in real-time adapts to the variations caused by the operational condition and battery condition.

In electronics, the lower cut-off voltage is the voltage at which the battery is fully discharged. At this voltage, the battery SoC is equal to 0 as follows:

$$V_{\text{low}} = V_{oc}|_{z=0} \approx V_{oc}|_{z=\delta} \approx a\log\delta + b + c \tag{22}$$

where V_{low} is the lower cut-off voltage of the battery, which is given in the battery specifications. Similarly, V_{oc} is equal to the higher cut-off voltage, V_{high}, when the battery is fully charged, as follows:

$$V_{\text{high}} = V_{oc}|_{z=1} = be + c \tag{23}$$

Subtract (22) from (23)

$$V_{\text{high}} - V_{\text{low}} = b(e-1) - a\log\delta \tag{24}$$

Solve for b as follows:

$$b = b(a) = \frac{\Delta V_{hl} + a\log\delta}{e-1} \tag{25}$$

where $\Delta V_{hl} = V_{\text{high}} - V_{\text{low}}$. Substitute (25) into (23), and solve for c as follows:

$$c = c(a) = V_{\text{high}} - b(a)e \tag{26}$$

The derivative of (21) with respect to z is

$$\frac{dV_{oc}}{dz} = \frac{a}{z} + 3be^{z^3}z^2 \tag{27}$$

Solve the equation for a

$$\begin{aligned} a &= \frac{f(dV_{oc}/dz, z)}{g(z,\delta)} \\ &= \frac{(dV_{oc}/dz)\, z\,(e-1) - 3\Delta V_{hl} e^{z^3} z^3}{(e-1) + 3e^{z^3}z^3\log\delta} \end{aligned} \tag{28}$$

The number of the parameter to be estimated for the SoC-OCV curve is reduced to 1, i.e., estimating a given by (28). The denominator of (28), $g(z,\delta)$, may approach zero depending upon z and δ and it would cause the numerical problem.

Algorithm 1 Calculation of $\tilde{a}_k$

1: Set $\epsilon > 0$, a small positive number
2: Calculate $g(\hat{z}_k, \delta) = (e-1) + 3e^{\hat{z}_k^3}\hat{z}_k^3\log\delta$
3: **if** $|g(\hat{z}_k, \delta)| < \epsilon$ **then**
4: Let $\hat{b}_k = \hat{b}_{k-1}$
5: Calculate $\tilde{a}_k$ from (27)
6: $\tilde{a}_k = \hat{z}_k(dV_{oc}/dz)_k - 3\hat{b}_k e^{\hat{z}_k^3}\hat{z}_k^3$
7: **else**
8: Calculate $\tilde{a}_k$ using (28)

Algorithm 1 is to prevent the numerical problem to calculate a. The current value of b is assumed to be constant for the neighbourhood of the singular point and (27) is used directly to calculate a. The calculated a in the algorithm denoted by $\tilde{a}_k$, is treated as the measurement in the estimation algorithm presented later.

To calculate (27) or (28), the OCV derivative with respect to the SoC is required. Providing the estimates of the OCV, $\hat{V}_{oc}$the following difference is calculated:

$$\Delta\hat{V}_{oc,k+1} = \hat{V}_{oc,k+1} - \hat{V}_{oc,k} \tag{29}$$

where $\hat{V}_{oc,k+1}$ and $\hat{V}_{oc,k}$ are provided by the KF designed in Algorithm 2. In addition, as the SoC propagation equation is given by [48]

$$z_{k+1} = z_k + \frac{I_k \Delta t_s}{C_{\max}} \tag{30}$$

where $C_{\max}$ is the battery capacity constant and Δt_s is the sampling time, the differential z at step $k+1$ is calculated as follows:

$$\Delta z_{k+1} = \frac{I_k \Delta t_s}{C_{\max}} \tag{31}$$

Therefore, the derivative can be approximated by the first-order difference as follows:

$$\left.\frac{dV_{oc}}{dz}\right|_{k+1} \approx \frac{\Delta \hat{V}_{oc,k+1}}{\Delta z_{k+1}} = \frac{\Delta \hat{V}_{oc,k+1} C_{\max}}{I_k \Delta t_s} \tag{32}$$

and the approximation with the current z are substituted into (28). Equation (21) is now written as a function of z only. Therefore, the estimation of z leads to the estimation of SoC-OCV curve.

The SoC estimation problem has the linear state propagation equation, (30), and the nonlinear measurement equation, (21). The EKF for estimation z, i.e., $\hat{z}$, is given in Algorithm 2, where the observation matrix is defined by the following Jacobian

$$H_k = \left.\frac{\partial V_{oc}}{\partial z}\right|_{z=\hat{z}_k, a=\hat{a}_k} = \frac{\hat{a}_k}{\hat{z}_k} + 3b(\hat{a}_k) e^{\hat{z}_k^3} \hat{z}_k^2 \tag{33}$$

where $\hat{a}_k$ is to be estimated.

The direct substitution of $\tilde{a}_k$ in Algorithm 1 into (33), however, would amplify undesirable noises in the measurements and the estimated values. Additional KF is designed for estimating a, where it is assumed that a varies slowly in each sampling interval, i.e.,

$$a_{k+1} = a_k + w_{a,k} \tag{34}$$

where $w_{a,k}$ is the process noise with the zero-mean and the variance equal to q_a. To apply the KF design procedure, $\tilde{a}_k$ from Algorithm 1 is treated as the measurement and assumed to have the following measurement noise characteristic:

$$\tilde{a}_k = a + v_{a,k} \tag{35}$$

where $\tilde{a}_k$ is the measurement of the true a. $v_{a,k}$ is the zero mean Gaussian measurement noise, which is independent to the process noise, $w_{a,k}$. To calculate the variance of $v_{a,k}$, $z_k^{(i)}$ samples are generated as follows:

$$z_k^{(i)} = \hat{z}_k + v_{z,k}^{(i)} \tag{36}$$

where $i = 1, 2, \ldots, N_s$, N_s is the number of samples and $v_{z,k}^i$ is the zero-mean Gaussian with the variance equal to $r_{z,k}$. The $\tilde{a}_k^{(i)}$ particles are calculated by substituting $z_k^{(i)}$ samples into Algorithm 1. The variance of $v_{a,k+1}$ is then calculated by the samples as follows:

$$r_{a,k} = \frac{\sum_{i=1}^{N_s} \left[\tilde{a}_k^{(i)} - \bar{a}_k\right]^2}{N_s - 1} \tag{37}$$

where $\bar{a}_k = \sum \tilde{a}_k^{(i)} / N_s$. Finally, the whole algorithm is summarized in Algorithm 2, where $(\cdot)_{k+1|k}$ is the priori prediction of $(\cdot)$ and $(\cdot)_{k+1|k+1}$ is the posteriori estimation of $(\cdot)$. Using separate KF algorithms to estimate OCV, coefficient a and SoC is recommended in order to reduce computational cost.

Algorithm 2 Adaptive SoC estimation algorithm

Initialise: $\hat{\theta}_0$, $\hat{\boldsymbol{x}}_0$, P_0, $\hat{z}_0$, $p_{z,0}$, $\hat{a}_0$ and $p_{a,0}$
while true **do**
  Obtain the measurement and input: $\tilde{V}_{t,k}$, I_k
  Run the parameter estimation using (14) & (15)
  Run **Algorithm 1** to obtain $\tilde{a}_k$
  Calculate the variance of $\tilde{a}_k$ using (36) & (37)
  Propagate
    $\hat{x}_{k+1|k} = A_k \hat{x}_{k|k} + B_k u_k$
    $P_{k+1|k} = A_k P_{k|k} A^T + Q$
    z using (30)
    $p_{z,k+1|k} = p_{z,k|k} + q_z$
    $\hat{a}_{k+1|k} = \hat{a}_{k|k}$
    $p_{a,k+1|k} = p_{a,k|k} + q_a$
  Update
    $L_{k+1} = P_{k+1|k} C_k^T / \left[C_k P_{k+1|k} C_k^T + r\right]$
    $\hat{x}_{k+1|k+1} = \hat{x}_{k+1|k} + L_{k+1}\left(\tilde{V}_t - \hat{V}_{t,k+1|k}\right)$
    $P_{k+1|k+1} = (1 - L_{k+1} C_k) P_{k+1|k}$
    $K_{z,k+1} = p_{z,k+1|k} H^T / (H p_{z,k+1|k} H^T + r_z)$
    $K_{a,k+1} = p_{a,k+1|k} / (p_{a,k+1|k} + r_{a,k+1})$
    $\hat{a}_{k+1|k+1} = \hat{a}_{k+1|k} + K_{a,k+1}\left(\tilde{a} - \hat{a}_{k+1|k}\right)$
    $p_{a,k+1|k+1} = (1 - K_{a,k+1}) p_{a,k+1|k}$
    $\hat{z}_{k+1|k+1} = \hat{z}_{k+1|k} + K_{z,k+1}\left(\tilde{V}_{oc} - \hat{V}_{oc,k+1|k}\right)$
    $p_{z,k+1|k+1} = (1 - K_{z,k+1} H) p_{z,k+1|k}$
  Repeat

VI. Numerical Simulations

A fully charged battery simulation was conducted to show the estimation results of our proposed algorithm. The simulated battery capacity is 0.85Ah. The discharge current rate is 1C. The simulated true values of R_0, R_p and C_p are chosen as 0.1Ω, 0.015Ω and 100F, respectively and these values are similar in [44] and [49]. For the simulation purpose, its nonlinear relation between SoC and V_{oc} is modelled as a rational function given by

$$V_{oc}(z) = \frac{\sum_{j=0}^{4} k_j z^j}{\sum_{j=0}^{4} q_j z^j} \tag{38}$$

where $k_0 = 16.65$, $k_1 = 516.2$, $k_2 = 519.9$, $k_3 = 5.696$, $k_4 = -4.523$, $q_0 = 2.591$, $q_1 = 70.68$, $q_2 = 61.26$, $q_3 = 14.07$, $q_4 = -24.92$. The initial unknown parameter vector is set to: $\hat{\boldsymbol{\theta}}_0 = [1, -0.05, 0.05]^T$. These initial values are similar in [50] and [51]. The initial V_{oc} and I_a are set to 7V and 0A, respectively. The covariance or the variance for OCV estimation are: $Q = 0.01 I_{2\times 2}$ and $r = 0.1$ [52], where $I_{2\times 2}$ is the 2×2 identity matrix.

The initial z estimate is set to 50% while the true is 100%. The initial p_z, p_a, r_z and r_a are set to 0.001. N_s is set to 100. The initial a is chosen as 0.5. The adaptive gain $\Gamma = 1000 I_{3x3}$. Δt_s is set to 0.01s. The higher cut-off voltage, V_{high}, is equal to 8.4756V and the lower cut-off voltage, V_{low}, is equal to 6.4735V. δ and ϵ are set to 0.001 and 0.1, respectively.

Figure 2 illustrates that the online parameter estimation algorithm provides accurate estimates of the parameters. R_0

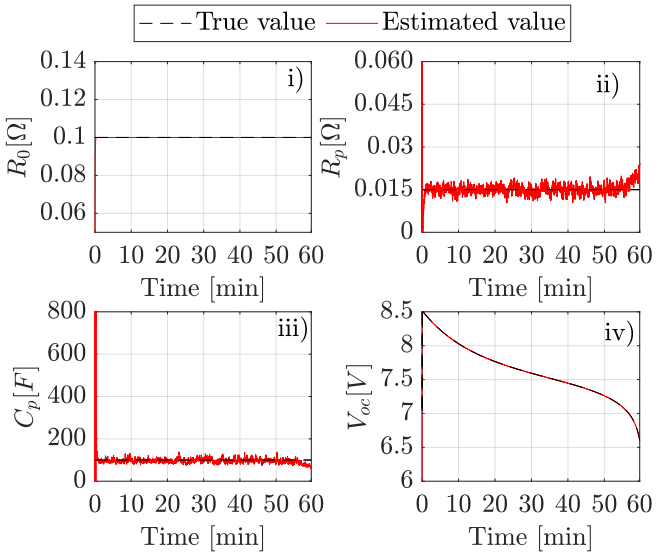

Fig. 2: Battery parameters & OCV estimation: i) Ohmic resistance, ii) Polarisation resistance, iii) Polarisation capacitance and iv) OCV

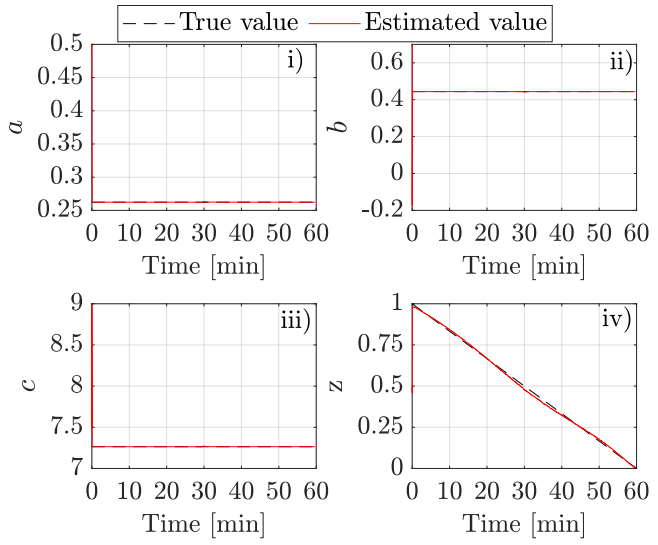

Fig. 3: SoC-OCV parameters & SoC estimation: i) Coefficient a, ii) Coefficient b, iii) Coefficient c, iv) SoC

converges fast to its true value whereas R_p and C_p show more fluctuations.

The calculated parameters are fed to the KF to estimate the V_{oc}. Figure 2 (iv) demonstrates that the fast convergence of the parameters leads to the fast convergence of V_{oc}. The estimated V_{oc} agrees with the true V_{oc} until the battery is fully discharged.

The SoC-OCV model parameters shown in Figure 3 (i-iii) and SoC shown in Figure 3 (iv) converge immediately. The SoC-OCV characteristic is dependent on the ambient temperature. When the ambient temperature is lower, the OCV becomes higher or vice versa, however, this behavior is not observed at high SoC regions, i.e. SoC $>$ 80%, [53], [54]. Figure 4 shows that the proposed model adequately represents

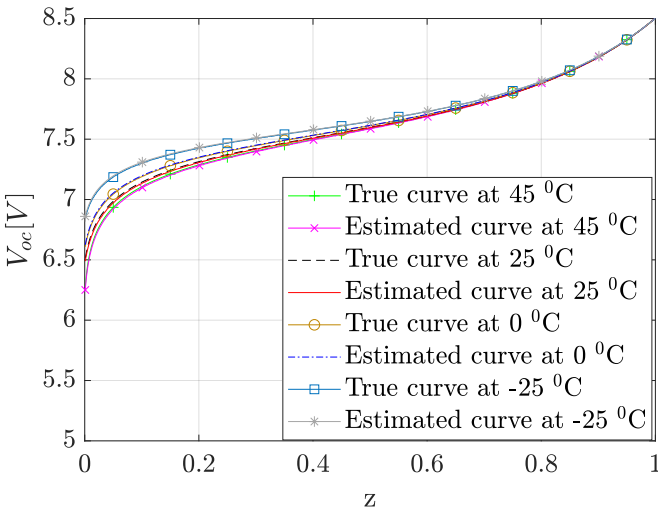

Fig. 4: Estimated & True SoC-OCV curves at different temperatures

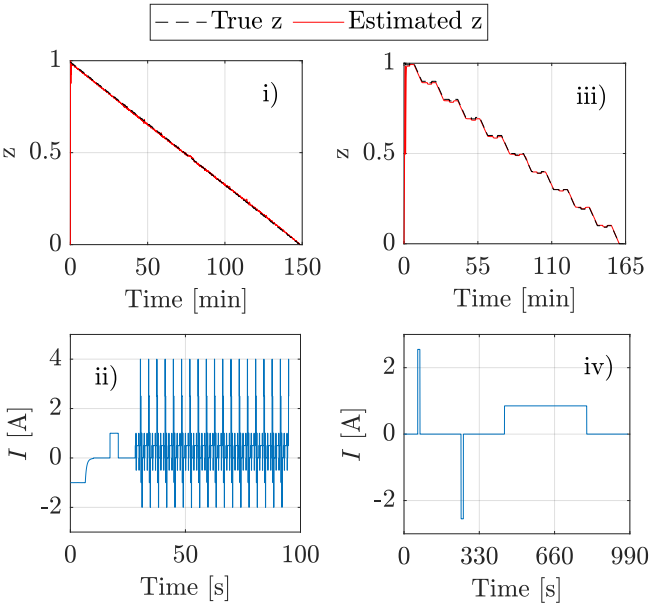

Fig. 5: SoC estimation results under dynamic loading: i) SoC estimation under DST profile, ii) DST test current profile, iii) SoC estimation under HPPC test profile, iv) HPPC test current profile

the nonlinear SoC-OCV relation and adapts to the curve variations at different temperatures.

Figure 5 shows the SoC estimation results under two different dynamic loading including dynamic stress test (DST) profile given in Figure 5 (ii) and hybrid pulse power characterisation (HPPC) test profile given in Figure 5 (iv). DST and HPPC test profiles are widely employed in evaluating the performance of SoC estimation algorithms used in EVs [55]. Figures 5 (i) and Figure 5 (iii) illustrate that the proposed algorithm robustly estimates the SoC under different dynamic loading.

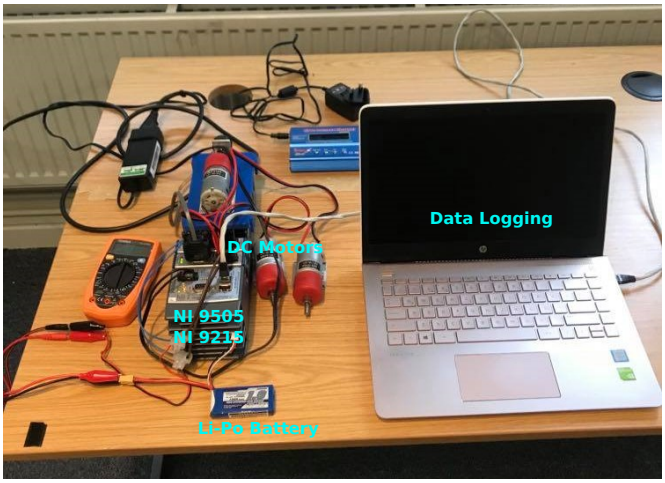

Fig. 6: The experimental setup

TABLE I: SoC-OCV relation obtained from SoC drop test

z	0	0.05	0.1	0.15	0.2
V_{oc} [V]	6.5688	7.2294	7.365	7.4088	7.4625
z	0.3	0.4	0.5	0.6	0.7
V_{oc} [V]	7.5363	7.5813	7.6401	7.7304	7.8663
z	0.8	0.85	0.9	0.95	1
V_{oc} [V]	8.0011	8.1325	8.2151	8.3038	8.3801

VII. Battery Experiment

A battery test rig shown in Figure 6 has been assembled by powering three DC motors by a LiPo battery in new condition. Its minimum capacity is given to be 1Ah by the manufacturer. The battery configuration has serially-connected two cells, each with a nominal voltage of 3.7V. The battery's peak discharge rate is 40C whereas its maximum charge rate is 2C. I and V_t are acquired through a NI 9505 and NI 9215 devices during the battery operation. A commercial battery charger has been used to charge the battery with a constant-current constant-voltage mode. The charger can also discharge the battery with a constant current. The upper cut-off voltage is set to be 8.4V to prevent possible damages to electrodes due to overcharging. Similarly, when the terminal voltage reaches lower cut-off voltage which is equal to 6.4V, the battery is considered as fully discharged. The room temperature is remained at 25°C ±3°C. The motor speed is remained at 50 rpm (revolutions per minute) thus the battery is discharged under constant current. All measured data are saved in every 0.01s.

A. Battery capacity

The battery capacity is given in the battery specification along with the lower and upper cut-off voltage values. However, the real capacity may be slightly different from the one given by the manufacturer. This might affect the SoC estimation accuracy. Hence, the experimental battery capacity is found by drawing a constant current, i.e., 1C, from the fully charged battery. When the battery reaches to the lower cut-off voltage value, it is considered to be completely discharged. During this process, the amount of the current drained from the battery and the time are measured. Therefore, the experimental capacity is simply calculated from the area under the time versus current graph. This procedure is repeated 5 times and the average capacity is calculated as 0.96Ah.

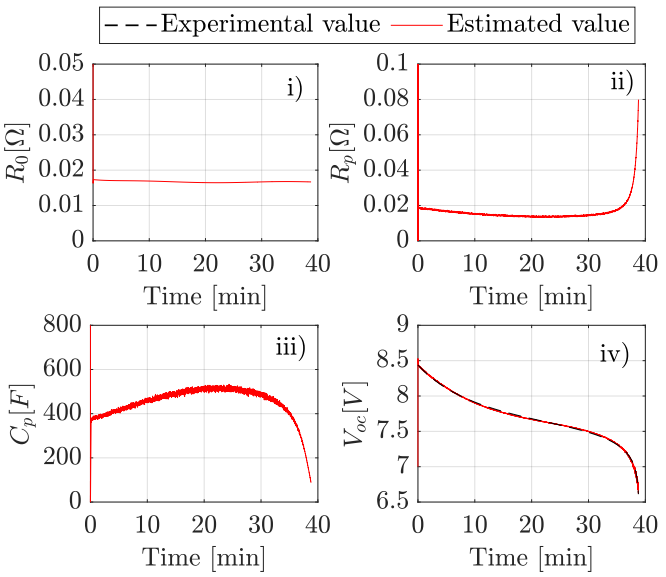

Fig. 7: LiPo battery's physical parameter & OCV estimation: i) Ohmic resistance, ii) Polarisation resistance, iii) Polarisation capacitance and iv) OCV

B. SoC-OCV relation

To establish the experimental SoC-OCV relation, the battery is fully charged under a constant-current constant-voltage mode until it reaches the upper cut-off voltage. Then, the battery is discharged by 5% intervals until SoC reaches 80%. The SoC drop interval is then increased to 10% until SoC reaches to 20%. The SoC drop rate is again decreased to 5% until the battery is fully discharged. This change in the SoC drop rate has been done to better capture the nonlinearity at low and high SoC regions. One hour relaxation period is used between the two discharging intervals. The terminal voltage measured after each resting period is assumed to be the V_{oc}. The SoC calculated using CC is considered as the reference SoC. The measured V_{oc} value is recorded with its corresponding SoC value. The same process is repeated for the battery charging process to take into account the differences in V_{oc} due to hysteresis. The average V_{oc} values are calculated and Table I is the look-up table for the experimentally obtained SoC and OCV relation.

C. Validation Experiment

Parameters of the ECM and coefficients of SoC-OCV curve are identified by Algorithm 2 from the experimental data of the LiPo battery. The same initial values as in the numerical simulation are used in the validation simulations. The fully charged battery is discharged by three DC motors. V_t and I are measured every 0.01s.

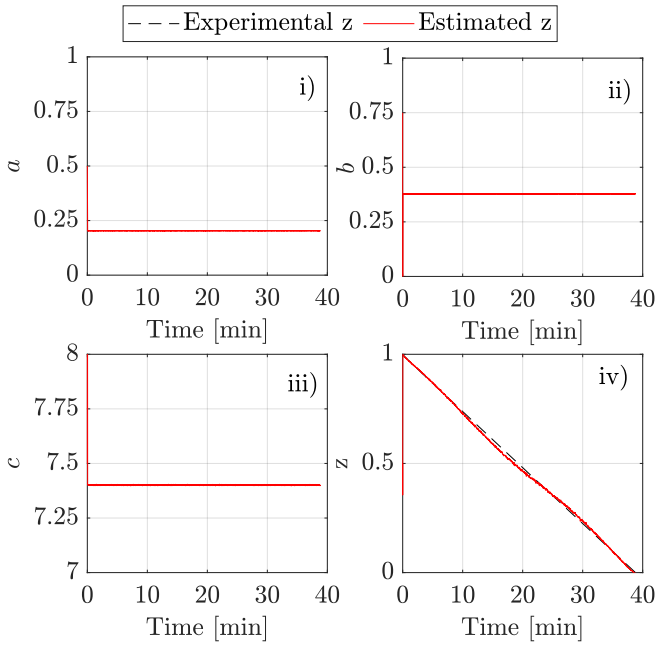

Fig. 8: Estimated Coefficients of SoC-OCV curve and estimated SoC compared to experimental SoC: i) Coefficient a, ii) Coefficient b, iii) Coefficient c, iv) SoC

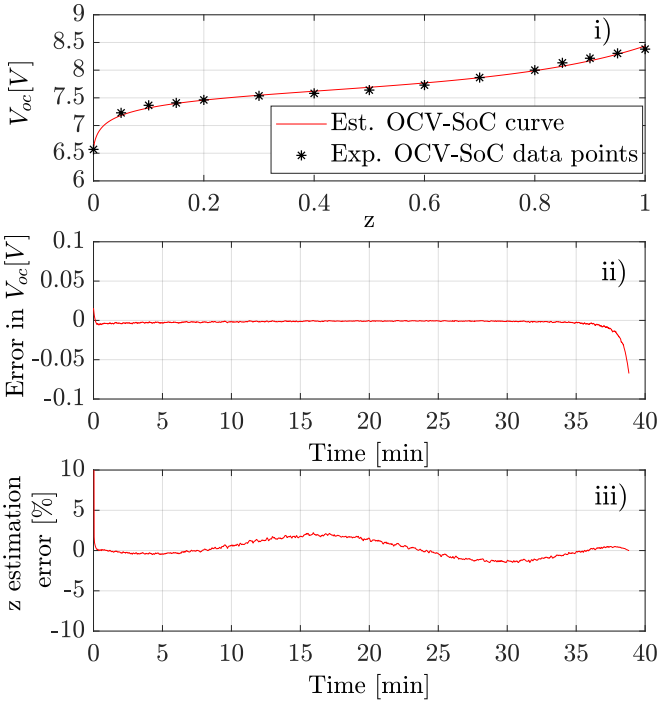

Fig. 9: Experimental SoC-OCV data points along with the estimated SoC-OCV curve & Estimation error in OCV and SoC: i) SoC-OCV curve, ii) Error in OCV, iii) Error in SoC

Figure 7 shows the convergence of the battery model parameters. All three model parameters converge almost immediately. The estimation of R_0 has a persistent trend around 0.18Ω. Note that the estimated R_0 includes the wiring resistance. On the other hand, R_p increases as the SoC decreases. It starts with around 0.02Ω and reaches around 0.08Ω at the end of discharging. C_p has the reverse trend compare to R_p. This is because the time constant of the battery tends to remain constant during the discharge process. Thus, C_p decreases to compensate the increase in R_p. The similar behaviours are also observed in [21], [56], [57].

Figure 7 (iv) shows the estimated V_{oc} in a solid red line whereas the experimental V_{oc} is in the dashed black line. The experimental V_{oc} is obtained from the data given in Table I. The estimated V_{oc} converges to the experimental V_{oc} less than 1s. The accuracy in V_{oc} estimation is requisite for the accurate estimation of SoC. The estimates of SoC-OCV curve coefficients are shown in Figure 8 (i-iii) and Figure 8 (iv) illustrates the SoC convergence. The SoC converges to its experimental value in less than 1s. It is vital to accurately estimate the SoC at low and high SoC values because it is necessary to know when to stop charging or discharging the battery. In these nonlinear regions, the estimated SoC agrees well with the experimental SoC as shown in Figure 8 (iv).

Figure 9 (i) shows the final SoC-OCV curve estimation in the red solid line, which is well aligned with the experimentally obtained data indicated by "*". Figure 9 (ii) illustrates the error in V_{oc} estimation. The V_{oc} estimation agrees well with the experimental V_{oc} within the maximum error ±0.1V. Figure 9 (iii) demonstrates the error in the SoC estimation. The error bound in z is within less than ±0.03.

The performance of the proposed algorithm shown with the experiment validates the capability of the algorithm to adapt to the noisy environment and measurement.

VIII. Conclusions and Future Work

The real-time SoC estimation algorithm is proposed based on a new SoC-OCV model. The physical battery parameters are estimated using the adaptive law. The OCV is estimated using the KF, the SoC is estimated using the EKF and another KF is used to develop the nonlinear curve estimation algorithm. The proposed algorithm is validated by performing the computer simulation and battery experiment. Both results validate that the proposed method provides an accurate estimation of SoC, and the experiment shows that the SoC estimation error is less than 2.5%.

The proposed method could be directly implemented for many applications including EVs. It eliminates all laborious time consuming experiments and reduces the SoC estimation error due to the inaccuracy in the SoC-OCV nonlinear curve obtained offline. Changes in the SoC-OCV curve by operational condition and battery ageing are automatically reflected in the estimation in real-time.

The future work will include robustness and sensitivity analysis of the proposed algorithm considering the drift noise in the input current measurement. Further computational and experimental research will be carried out on the accuracy of the approximation model given in Eq. (21) for different battery types. Moreover, the behaviour of the SoC estimation error due to the difference between the model and the truth will be investigated by realistic and extreme condition experiments.

ACKNOWLEDGMENTS

The authors would like to thank the Republic of Türkiye Ministry of National Education for funding support for the first author's PhD at the University of Leeds.

AUTHORS' CONTRIBUTIONS

O. Kadem: Algorithm design and implementation, performing the computer simulation and battery experiment, writing original draft, review, editing. J. Kim: Algorithm design, writing, review, editing, supervision.

DATA AVAILABILITY

Data available on request from the authors.

REFERENCES

[1] S. Manzetti and F. Mariasiu, "Electric vehicle battery technologies: From present state to future systems," *Renewable and Sustainable Energy Reviews*, vol. 51, pp. 1004 – 1012, 2015. [Online]. Available: http://www.sciencedirect.com/science/article/pii/S1364032115006577

[2] M. Thackeray, C. Wolverton, and E. Isaacs, "Electrical energy storage for transportation approaching the limits of, and going beyond, lithium-ion batteries," *Energy and Environmental Science*, vol. 5, pp. 7854–7863, 2012.

[3] L. H. Saw, Y. Ye, and A. A. Tay, "Integration issues of lithium-ion battery into electric vehicles battery pack," *Journal of Cleaner Production*, vol. 113, pp. 1032–1045, 2016. [Online]. Available: https://www.sciencedirect.com/science/article/pii/S0959652615016406

[4] Z. Wang, C. Song, L. Zhang, Y. Zhao, P. Liu, and D. G. Dorrell, "A data-driven method for battery charging capacity abnormality diagnosis in electric vehicle applications," *IEEE Transactions on Transportation Electrification*, vol. 8, no. 1, pp. 990–999, 2022.

[5] C. She, L. Zhang, Z. Wang, F. Sun, P. Liu, and C. Song, "Battery state of health estimation based on incremental capacity analysis method: Synthesizing from cell-level test to real-world application," *IEEE Journal of Emerging and Selected Topics in Power Electronics*, pp. 1–1, 2021.

[6] L. He and D. Guo, "An improved coulomb counting approach based on numerical iteration for soc estimation with real-time error correction ability," *IEEE Access*, vol. 7, pp. 74 274–74 282, 2019.

[7] B. Jenkins, A. Krupadanam, and A. Annaswamy, "Fast adaptive observers for battery management systems," *IEEE Transactions on Control Systems Technology*, vol. PP, pp. 1–14, 02 2019.

[8] R. Xiong, J. Cao, Q. Yu, H. He, and F. Sun, "Critical review on the battery state of charge estimation methods for electric vehicles," *IEEE Access*, vol. 6, pp. 1832–1843, 2018.

[9] K. S. Ng, C.-S. Moo, Y.-P. Chen, and Y.-C. Hsieh, "Enhanced coulomb counting method for estimating state-of-charge and state-of-health of lithium-ion batteries," *Applied Energy*, vol. 86, no. 9, pp. 1506 – 1511, 2009. [Online]. Available: http://www.sciencedirect.com/science/article/pii/S0306261908003061

[10] A. Wadi, M. F. Abdel-Hafez, and A. A. Hussein, "Mitigating the effect of noise uncertainty on the online state-of-charge estimation of li-ion battery cells," *IEEE Transactions on Vehicular Technology*, vol. 68, no. 9, pp. 8593–8600, 2019.

[11] A. Farmann, W. Waag, A. Marongiu, and D. U. Sauer, "Critical review of on-board capacity estimation techniques for lithium-ion batteries in electric and hybrid electric vehicles," *Journal of Power Sources*, vol. 281, pp. 114 – 130, 2015. [Online]. Available: http://www.sciencedirect.com/science/article/pii/S0378775315001457

[12] J. Shen, J. Shen, Y. He, and Z. Ma, "Accurate state of charge estimation with model mismatch for li-ion batteries: A joint moving horizon estimation approach," *IEEE Transactions on Power Electronics*, vol. 34, no. 5, pp. 4329–4342, 2019.

[13] M. Doyle, T. F. Fuller, and J. Newman, "Modeling of galvanostatic charge and discharge of the lithium/polymer/insertion cell," *Journal of The Electrochemical Society*, vol. 140, no. 6, pp. 1526–1533, jun 1993. [Online]. Available: https://doi.org/10.1149%2F1.2221597

[14] J. S. Newman and K. E. Thomas-Alyea, *Electrochemical systems / John Newman and Karen E. Thomas-Alyea.*, 3rd ed. Hoboken, N.J.: J. Wiley, 2004.

[15] N. Baba, H. Yoshida, M. Nagaoka, C. Okuda, and S. Kawauchi, "Numerical simulation of thermal behavior of lithium-ion secondary batteries using the enhanced single particle model," *Journal of Power Sources*, vol. 252, pp. 214 – 228, 2014. [Online]. Available: http://www.sciencedirect.com/science/article/pii/S037877531301954X

[16] M. Guo, G. Sikha, and R. White, "Single-particle model for a lithium-ion cell: Thermal behavior (vol 158, pg a122, 2011)," *Journal of The Electrochemical Society*, vol. 158, 01 2011.

[17] Z. Pei, X. Zhao, H. Yuan, Z. Peng, and L. wu, "An equivalent circuit model for lithium battery of electric vehicle considering self-healing characteristic," *Journal of Control Science and Engineering*, vol. 2018, pp. 1–11, 06 2018.

[18] A.-I. Stroe, J. Meng, D.-I. Stroe, M. Świerczyński, R. Teodorescu, and S. Kær, "Influence of battery parametric uncertainties on the state-of-charge estimation of lithium titanate oxide-based batteries," *Energies*, vol. 11, p. 795, 03 2018.

[19] J. Du, Z. Chen, and F. Li, "Multi-objective optimization discharge method for heating lithium-ion battery at low temperatures," *IEEE Access*, vol. 6, pp. 44 036–44 049, 2018.

[20] M. Hossain, S. Saha, M. T. Arif, A. M. T. Oo, N. Mendis, and M. E. Haque, "A parameter extraction method for the li-ion batteries with wide-range temperature compensation," *IEEE Transactions on Industry Applications*, vol. 56, no. 5, pp. 5625–5636, 2020.

[21] X. Liu, Y. Jin, S. Zeng, X. Chen, Y. Feng, S. Liu, and H. Liu, "Online identification of power battery parameters for electric vehicles using a decoupling multiple forgetting factors recursive least squares method," *CSEE Journal of Power and Energy Systems*, vol. 6, no. 3, pp. 735–742, 2020.

[22] H. He, R. Xiong, X. Zhang, F. Sun, and J. Fan, "State-of-charge estimation of the lithium-ion battery using an adaptive extended kalman filter based on an improved thevenin model," *IEEE Transactions on Vehicular Technology*, vol. 60, no. 4, pp. 1461–1469, 2011.

[23] R. Xiong, H. He, F. Sun, and K. Zhao, "Evaluation on state of charge estimation of batteries with adaptive extended kalman filter by experiment approach," *IEEE Transactions on Vehicular Technology*, vol. 62, no. 1, pp. 108–117, 2013.

[24] X. Wu, X. Li, and J. Du, "State of charge estimation of lithium-ion batteries over wide temperature range using unscented kalman filter," *IEEE Access*, vol. 6, pp. 41 993–42 003, 2018.

[25] V. Sangwan, R. Kumar, and A. Kumar Rathore, "State-of-charge estimation of li-ion battery at different temperatures using particle filter," *The Journal of Engineering*, vol. 2019, no. 18, pp. 5320–5324, 2019.

[26] D. Zhou, K. Zhang, A. Ravey, F. Gao, and A. Miraoui, "Online estimation of lithium polymer batteries state-of-charge using particle filter-based data fusion with multimodels approach," *IEEE Transactions on Industry Applications*, vol. 52, no. 3, pp. 2582–2595, 2016.

[27] M. Partovibakhsh and G. Liu, "An adaptive unscented kalman filtering approach for online estimation of model parameters and state-of-charge of lithium-ion batteries for autonomous mobile robots," *IEEE Transactions on Control Systems Technology*, vol. 23, no. 1, pp. 357–363, 2015.

[28] D. Liu, X. Yin, Y. Song, W. Liu, and Y. Peng, "An on-line state of health estimation of lithium-ion battery using unscented particle filter," *IEEE Access*, vol. 6, pp. 40 990–41 001, 2018.

[29] Q. Ouyang, J. Chen, and J. Zheng, "State-of-charge observer design for batteries with online model parameter identification: A robust approach," *IEEE Transactions on Power Electronics*, vol. 35, no. 6, pp. 5820–5831, 2020.

[30] H. Rahimi-Eichi, F. Baronti, and M. Chow, "Online adaptive parameter identification and state-of-charge coestimation for lithium-polymer battery cells," *IEEE Transactions on Industrial Electronics*, vol. 61, no. 4, pp. 2053–2061, 2014.

[31] P. Shen, M. Ouyang, L. Lu, J. Li, and X. Feng, "The co-estimation of state of charge, state of health, and state of function for lithium-ion batteries in electric vehicles," *IEEE Transactions on Vehicular Technology*, vol. 67, no. 1, pp. 92–103, 2018.

[32] H. Chaoui, N. Golbon, I. Hmouz, R. Souissi, and S. Tahar, "Lyapunov-based adaptive state of charge and state of health estimation for lithium-ion batteries," *IEEE Transactions on Industrial Electronics*, vol. 62, no. 3, pp. 1610–1618, 2015.

[33] Y. Zheng, M. Ouyang, X. Han, L. Lu, and J. Li, "Investigating the error sources of the online state of charge estimation methods for lithium-ion batteries in electric vehicles," *Journal of Power Sources*, vol. 377, pp. 161–188, 2018. [Online]. Available: https://www.sciencedirect.com/science/article/pii/S037877531731594X

[34] I. Jokić, Ž. Zečević, and B. Krstajić, "State-of-charge estimation of lithium-ion batteries using extended kalman filter and unscented kalman

filter," in *2018 23rd International Scientific-Professional Conference on Information Technology (IT)*, 2018, pp. 1–4.
[35] H. Aung, K. Soon Low, and S. Ting Goh, "State-of-charge estimation of lithium-ion battery using square root spherical unscented kalman filter (sqrt-ukfst) in nanosatellite," *IEEE Transactions on Power Electronics*, vol. 30, no. 9, pp. 4774–4783, 2015.
[36] M. Shehab El Din, A. A. Hussein, and M. F. Abdel-Hafez, "Improved battery soc estimation accuracy using a modified ukf with an adaptive cell model under real ev operating conditions," *IEEE Transactions on Transportation Electrification*, vol. 4, no. 2, pp. 408–417, 2018.
[37] V. Knap and D.-I. Stroe, "Effects of open-circuit voltage tests and models on state-of-charge estimation for batteries in highly variable temperature environments: Study case nano-satellites," *Journal of Power Sources*, vol. 498, p. 229913, 2021. [Online]. Available: https://www.sciencedirect.com/science/article/pii/S0378775321004444
[38] X. Shu, G. Li, J. Shen, W. Yan, Z. Chen, and Y. Liu, "An adaptive fusion estimation algorithm for state of charge of lithium-ion batteries considering wide operating temperature and degradation," *Journal of Power Sources*, vol. 462, p. 228132, 2020. [Online]. Available: https://www.sciencedirect.com/science/article/pii/S0378775320304353
[39] Y. Song, M. Park, M. Seo, and S. W. Kim, "Improved soc estimation of lithium-ion batteries with novel soc-ocv curve estimation method using equivalent circuit model," in *2019 4th International Conference on Smart and Sustainable Technologies (SpliTech)*, 2019, pp. 1–6.
[40] B. R. Dewangga, S. Herdjunanto, and A. Cahyadi, "Battery current estimation based on simple model with parameter update strategy using piecewise linear soc-ocv," in *2018 4th International Conference on Science and Technology (ICST)*, 2018, pp. 1–6.
[41] M. Gholizadeh and F. Salmasi, "Estimation of state of charge, unknown nonlinearities, and state of health of a lithium-ion battery based on a comprehensive unobservable model," *Industrial Electronics, IEEE Transactions on*, vol. 61, pp. 1335–1344, 03 2014.
[42] J. Kim, J. Shin, C. Chun, and B. H. Cho, "Stable configuration of a li-ion series battery pack based on a screening process for improved voltage/soc balancing," *IEEE Transactions on Power Electronics*, vol. 27, no. 1, pp. 411–424, 2012.
[43] Min Chen and G. A. Rincon-Mora, "Accurate electrical battery model capable of predicting runtime and i-v performance," *IEEE Transactions on Energy Conversion*, vol. 21, no. 2, pp. 504–511, 2006.
[44] I. Jarraya, F. Masmoudi, M. H. Chabchoub, and H. Trabelsi, "An online state of charge estimation for lithium-ion and supercapacitor in hybrid electric drive vehicle," *Journal of Energy Storage*, vol. 26, p. 100946, 2019. [Online]. Available: https://www.sciencedirect.com/science/article/pii/S2352152X19303093
[45] M. Kwak, B. Lkhagvasuren, J. Park, and J. You, "Parameter identification and soc estimation of a battery under the hysteresis effect," *IEEE Transactions on Industrial Electronics*, vol. 67, no. 11, pp. 9758–9767, 2020.
[46] H. Chaoui and H. Gualous, "Adaptive state of charge estimation of lithium-ion batteries with parameter and thermal uncertainties," *IEEE Transactions on Control Systems Technology*, vol. 25, no. 2, pp. 752–759, 2017.
[47] P. Ioannou and B. Fidan, *Adaptive Control Tutorial*. Philadelphia, PA: Society for Industrial and Applied Mathematics, 2006. [Online]. Available: https://epubs.siam.org/doi/abs/10.1137/1.9780898718652
[48] T. Ouyang, P. Xu, J. Chen, J. Lu, and N. Chen, "An online prediction of capacity and remaining useful life of lithium-ion batteries based on simultaneous input and state estimation algorithm," *IEEE Transactions on Power Electronics*, vol. 36, no. 7, pp. 8102–8113, 2021.
[49] S. Wang, C. Fernandez, L. Shang, Z. Li, and J. Li, "Online state of charge estimation for the aerial lithium-ion battery packs based on the improved extended kalman filter method," *Journal of Energy Storage*, vol. 9, pp. 69–83, 2017. [Online]. Available: https://www.sciencedirect.com/science/article/pii/S2352152X16301608
[50] Y. Song, M. Park, M. Seo, and S. W. Kim, "Online state-of-charge estimation for lithium-ion batteries considering model inaccuracies under time-varying current conditions," *IEEE Access*, vol. 8, pp. 192 419–192 434, 2020.
[51] J. Xu, B. Cao, Z. Chen, and Z. Zou, "An online state of charge estimation method with reduced prior battery testing information," *International Journal of Electrical Power & Energy Systems*, vol. 63, pp. 178–184, 2014. [Online]. Available: https://www.sciencedirect.com/science/article/pii/S0142061514003664
[52] G. L. Plett, "Extended kalman filtering for battery management systems of lipb-based hev battery packs: Part 1. background," *Journal of Power Sources*, vol. 134, no. 2, pp. 252–261, 2004. [Online]. Available: https://www.sciencedirect.com/science/article/pii/S0378775304003593
[53] R. Zhang, B. Xia, B. Li, L. Cao, Y. Lai, W. Zheng, H. Wang, W. Wang, and M. Wang, "A study on the open circuit voltage and state of charge characterization of high capacity lithium-ion battery under different temperature," *Energies*, vol. 11, no. 9, 2018. [Online]. Available: https://www.mdpi.com/1996-1073/11/9/2408
[54] E. Choi and S. Chang, "A temperature-dependent state of charge estimation method including hysteresis for lithium-ion batteries in hybrid electric vehicles," *IEEE Access*, vol. 8, pp. 129 857–129 868, 2020.
[55] R. Xiong, J. Huang, Y. Duan, and W. Shen, "Enhanced lithium-ion battery model considering critical surface charge behavior," *Applied Energy*, vol. 314, p. 118915, 2022. [Online]. Available: https://www.sciencedirect.com/science/article/pii/S0306261922003373
[56] X. Du, J. Meng, Y. Zhang, X. Huang, S. Wang, P. Liu, and T. Liu, "An information appraisal procedure: Endows reliable online parameter identification to lithium-ion battery model," *IEEE Transactions on Industrial Electronics*, vol. 69, no. 6, pp. 5889–5899, 2022.
[57] W. Zhang, L. Wang, L. Wang, C. Liao, and Y. Zhang, "Joint state-of-charge and state-of-available-power estimation based on the online parameter identification of lithium-ion battery model," *IEEE Transactions on Industrial Electronics*, vol. 69, no. 4, pp. 3677–3688, 2022.